

Spectral function of the one-dimensional Hubbard model away from half filling

H. Benthien and F. Gebhard

Fachbereich Physik, Philipps-Universität, D-35032 Marburg, Germany

E. Jeckelmann

Institut für Physik, Johannes Gutenberg-Universität, D-55099 Mainz, Germany

(Dated: March 22, 2024)

We calculate the photoemission spectral function of the one-dimensional Hubbard model away from half filling using the dynamical density matrix renormalization group method. An approach for calculating momentum-dependent quantities in infinite open chains is presented. Comparison with exact Bethe Ansatz results demonstrates the unprecedented accuracy of our method. Our results show that the photoemission spectrum of the quasi-one-dimensional conductor TTF-TCNQ provides evidence for spin-charge separation on the scale of the conduction bandwidth.

PACS numbers: 71.10.Fd, 71.10.Pm, 79.60.Fr, 71.20.Rv

The Luttinger liquid theory describes the ground state and asymptotic low energy properties of one-dimensional correlated metals [1]. Two characteristics of a Luttinger liquid are the absence of quasiparticles predicted by the Fermi liquid theory of normal metals and the occurrence of independent spin and charge excitations. In principle, these features can be observed in the spectral function [2, 3] which corresponds to the spectrum measured in angle-resolved photoemission spectroscopy (ARPES) experiments. In real materials, however, the low-energy properties are likely to be governed by three-dimensional physics. One-dimensional physics is observed only above a crossover energy scale, even in the most strongly anisotropic materials. Consequently, it has proven difficult to observe unambiguous evidence for Luttinger liquid physics in experiments probing only low-energy properties of quasi-one-dimensional conductors.

A recent ARPES experiment for the quasi-one-dimensional organic conductor TTF-TCNQ (tetrathiafulvalene tetracyanoquinodimethane) has revealed significant discrepancies from the predictions of Fermi liquid theory and conventional electronic structure calculations [4, 5]. The experimental spectrum dispersion can be consistently mapped over the scale of the conduction bandwidth onto separated spin and charge excitation bands of the one-dimensional Hubbard model [6] away from half filling. This is one of the strongest pieces of experimental evidence for spin-charge separation and thus for Luttinger liquid physics in low-dimensional materials. However, a direct comparison of the experimental ARPES spectrum with the Hubbard model spectral function has not been possible yet.

The Hubbard model was solved exactly 36 years ago [7] and the dispersion of its excitation bands can be computed [8]. Nevertheless, the photoemission spectral function can only be calculated exactly in the limiting cases of noninteracting electrons or in infinitely strong electron interaction [9, 10] and in the low-energy limit described by the Luttinger liquid theory. Various numerical methods

have provided a qualitative picture of spectral functions in the Hubbard model but exact diagonalizations [10, 11] are limited to too small systems to investigate the thermodynamic limit while other approaches [12, 13] are based on various approximations of uncertain accuracy.

We have determined the photoemission spectral function of the one-dimensional Hubbard model with parameters appropriate for TTF-TCNQ using the dynamical density-matrix renormalization group (DDMRG) method [14]. A novel approach is used to calculate momentum-dependent quantities in infinite open chains. This allows us to investigate large systems almost exactly and to make a direct comparison of the Hubbard model spectral weight distribution with the experimental TTF-TCNQ spectrum. To demonstrate the accuracy of our method and to identify excitations contributing to the photoemission spectral function we compare our numerical results with exact Bethe Ansatz results.

A minimal model to describe the electronic properties of TTF-TCNQ is the one-dimensional Hubbard model defined by the Hamiltonian

$$\hat{H} = -t \sum_{l=1}^L \sum_{\sigma} \hat{c}_{l,\sigma}^\dagger \hat{c}_{l+1,\sigma} + \hat{c}_{l+1,\sigma}^\dagger \hat{c}_{l,\sigma} + U \sum_{l=1}^L \hat{n}_{l,\uparrow} \hat{n}_{l,\downarrow} \quad (1)$$

Here $\hat{c}_{l,\sigma}^\dagger$, $\hat{c}_{l,\sigma}$ are creation and annihilation operators for electrons with spin $\sigma = \uparrow, \downarrow$ at site $l = 1, \dots, L$ (representing a π -type Wannier orbital centered on a TCNQ molecule), $\hat{n}_{l,\sigma} = \hat{c}_{l,\sigma}^\dagger \hat{c}_{l,\sigma}$, and $\hat{n}_l = \hat{n}_{l,\uparrow} + \hat{n}_{l,\downarrow}$. Appropriate parameters for TTF-TCNQ are an on-site Coulomb repulsion $U = 4.9t$ and a hopping integral $t = 0.4eV$ [4, 5]. (These values are appropriate for the TTF-TCNQ surface, which is probed in ARPES experiments, not for bulk TTF-TCNQ.) Although the filling of the TCNQ band is $n = 0.59$, we use a slightly different filling $n = 0.6$ in our simulations to facilitate the finite-size-scaling analysis. For a chain with L sites and

$N = nL$ electrons the chemical potential is chosen so that $E_0(N-1) = E_0(N+1)$, where $E_0(N-1)$ is the ground state energy with $N-1$ electrons. Thus the Fermi energy is $\epsilon_F = 0$ in the thermodynamic limit $L \rightarrow \infty$.

The photoemission spectral function $A(k; \omega)$ is the imaginary part of the one-particle Green's function

$$A(k; \omega) = \frac{1}{\pi} \text{Im} \langle \langle \hat{c}_{k, \sigma}^{\dagger} | \frac{1}{\hat{H} - \epsilon_0 - i0^+} \hat{c}_{k, \sigma} | j_0 \rangle \rangle \quad (2)$$

where $|j_0\rangle$ and ϵ_0 are the ground state wavefunction and energy of the Hamiltonian (1). This function can be calculated for finite broadening and system sizes L using the dynamical DMRG method [14]. The spectral properties in the thermodynamic limit can be determined using a finite-size-scaling analysis [14] with an appropriate broadening (L). Here we have used $L = 9t$ and system sizes up to $L = 150$ sites. DMRG truncation errors are negligible for all results presented here (up to $m = 400$ density-matrix eigenstates have been kept per block in our calculations.)

The operators $\hat{c}_{k, \sigma}$ are usually defined using Bloch states [i.e., the one-electron eigenstates of the Hamiltonian (1) with periodic boundary conditions $\hat{c}_{L+1, \sigma} = \hat{c}_{1, \sigma}$ in the non-interacting limit ($U = 0$): $\hat{c}_{k, \sigma} = \frac{1}{\sqrt{L}} \sum_{j=1}^L e^{ikj} \hat{c}_{j, \sigma}$ with momentum $k = 2\pi z/L$ for integers $L/2 < z \leq L/2$. Since DMRG calculations can be performed for much larger system sizes using open boundary conditions, it is desirable to extend the definition of the spectral function $A(k; \omega)$ to that case. Therefore, we use the eigenstates of the particle-in-a-box problem [i.e., the one-electron eigenstates of the Hamiltonian (1) on an open chain for $U = 0$] to define the operators

$$\hat{c}_{k, \sigma} = \frac{1}{\sqrt{L+1}} \sum_{j=1}^L \sin(kj) \hat{c}_{j, \sigma} \quad (3)$$

with (quasi-)momentum $k = \pi z/(L+1)$ for integers $1 \leq z \leq L$. Both definitions of $\hat{c}_{k, \sigma}$ should be equivalent in the thermodynamic limit $L \rightarrow \infty$. Tests for finite systems up to $L = 32$ sites show that both approaches are consistent except in the asymptotic Luttinger liquid regime [i.e., at low energy ($|\omega| \ll t$) close to the Fermi vector $k_F = \pi/2$ ($k = k_F \pm \pi/(L+1)$)]. Therefore, open chains and the definition (3) can be used to investigate the spectral function $A(k; \omega)$. In this paper we present only results obtained using this approach.

Figures 1 and 2 show the spectral function calculated with DDMRG in a chain with $L = 90$ sites. Since the spectrum is symmetric, $A(k; \omega) = A(k; -\omega)$, we show results for $k \geq 0$ only. Three dispersing features are clearly visible in the spectrum for $k < k_F$ in Fig 1. At small binding energy $|\omega|$ there are intense peaks with a narrow dispersion (from $|\omega| = 0$ at $k = k_F$ to $|\omega| = 0.5t$ at $k = 0$). This feature corresponds to the spinon branches in the Luttinger liquid regime. Note that both spinon branches (for $k < 0$ and $k > 0$) join at $k = 0$ and

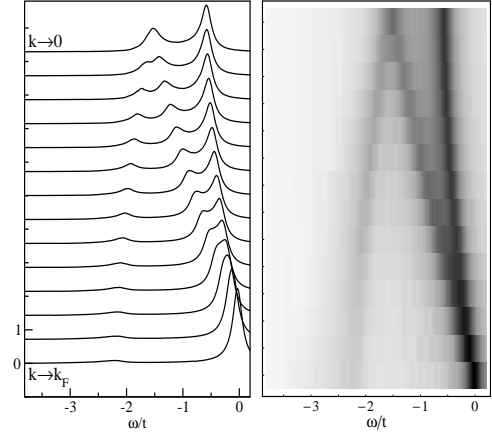


FIG. 1: Line shapes (left) and gray-scale plot (right) of the spectral function $A(k; \omega)$ for $0 < k < k_F$ calculated with a broadening $\gamma = 0.1t$ using DDMRG.

thus form just one spinon band. At energies $|\omega|$ lower than the spinon band there is a second spectral feature made of peaks with less spectral weight and a wider dispersion (from $|\omega| = 0$ at $k = k_F$ to $|\omega| = 1.5t$ at $k = 0$). It merges with the spinon band for $k \rightarrow k_F$ because of the finite broadening. This feature corresponds to the two holon branches of the Luttinger liquid theory. The third spectral feature is made of weaker peaks and has an (apparently) inverted dispersion (starting at $|\omega| = 1.5t$ for $k = 0$ and reaching $|\omega| = 2.2t$ at $k = k_F$). These so-called shadow bands [9] are actually the continuation of the holon bands. Thus the second and third features correspond to two holon/shadow bands crossing at $k = 0$. While the spectral weight of the structure associated with the spinon and holon bands remains relatively constant for all $k < k_F$, the shadow bands rapidly lose intensity with increasing k .

For $k > k_F$ the spectral weight is much lower than for $k < k_F$ (see Fig. 2). Nevertheless, one can observe four dispersive structures in the spectral function. First, the shadow band continues from $k = k_F$ to $3k_F$, but its energy increases with k and approaches zero for $k \rightarrow 3k_F$. Weaker peaks are also visible at higher energy $|\omega|$ than the shadow band for $k_F < k < 2k_F$. The corresponding binding energy $|\omega|$ increases from about zero at $k = k_F$ to about $1.7t$ at $k = 2k_F$, where this second feature meets the shadow band and apparently disappears. The third dispersing feature corresponds to very weak peaks (not visible on the scale of Fig. 2) with energies from $|\omega| = 3.7t$ at $k = 0$ to $|\omega| = 2.2t$ at $k = 2k_F$. Note that, despite its weakness, this feature corresponds to the spectrum maximum for $k = 0$. The last feature is a sharp drop of the spectral weight at low energy. It goes from $|\omega| = 3.25t$ at $k = k_F$ to $|\omega| = 4.6t$ at $k = 0$. We interpret this drop as the lower edge of the photoemission spectrum. The little spectral weight found at lower energy $|\omega|$ is due to the finite broadening

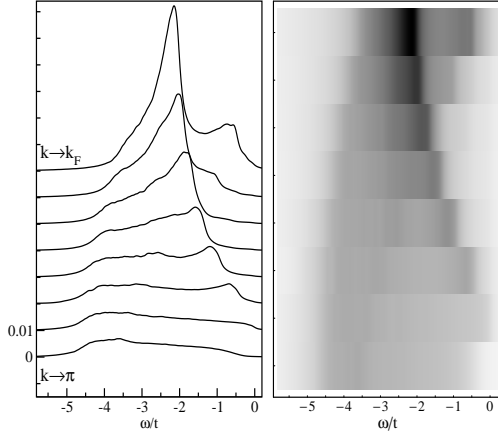


FIG. 2: Line shapes (left) and gray-scale plot (right) of the spectral function $A(k;!)$ for $k_F < k <$ calculated with a broadening $= 0.1t$ using DDMRG.

used in our DDMRG calculations. Note that these third and fourth spectral features are not visible for small $|k_j|$ because they are too close to the broadened and comparably much stronger peaks belonging to other structures.

Figure 3 shows the dispersion $! (k)$ of the various features found in the DDMRG spectrum for the 90-site chain. One clearly sees that the shadow bands are just the continuation of the holon bands. The dispersions $! (k)$ should naturally correspond to specific excitation bands $! (k)$ of the Hubbard model. To identify these excitations we have calculated the excitation energies $! (k)$ for the removal of an electron in the Hubbard model on a 90-site chain using the Bethe Ansatz solution [8]. In Fig. 3 we show those excitation bands $! (k)$ which correspond to the dispersing features found in the DDMRG spectral function. The excellent quantitative agreement between the Bethe Ansatz results calculated for periodic boundary conditions and our numerical data confirms that the open chains used in our DDMRG calculations do not affect the spectral properties significantly.

Due to the separation of spin and charge dynamics, electron-removal excitations with momentum k are made of independent spin and charge excitations with momenta k_s and $k_c = k - k_s$, respectively. The spinon band between $-k_F$ and k_F is related to excitations with the lowest possible binding energy for $k_c = 0$ and $|k_s| < k_F$. This defines the spinon dispersion $!_s(k_s)$, which has a width of about $0.5t$ and gives the spectral onset for $|k_j| < k_F$. The holon/shadow bands going from $-k_F$ to $3k_F$ and from

$3k_F$ to k_F correspond to excitations with the lowest possible binding energy for $|k_s| = k_F$, $0 < |k_c| < 4k_F$, and $k_s k_c < 0$. This defines the holon dispersion $!_c(k_c)$ with a width of about $2t$. It gives the spectral onset for $2k_F < |k_j| < 3k_F$. The peaks found at low binding energy for $k_F < |k_j| < 2k_F$ correspond to secondary holon bands made of similar excitations as the holon-shadow bands but with parallel spin and charge momenta ($k_s k_c > 0$).

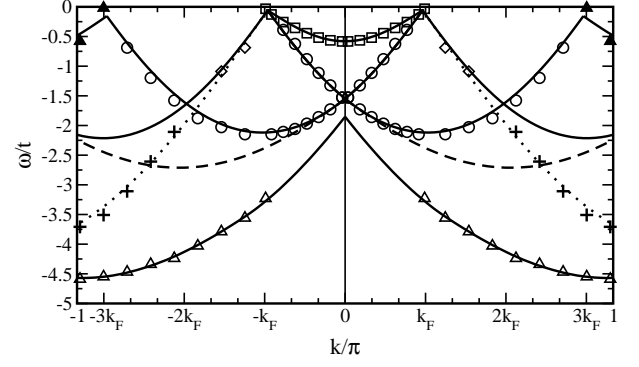


FIG. 3: Dispersion $! (k)$ of the structures observed in the DDMRG spectral function: spinon band (square), holon-shadow bands (circle), secondary holon bands (diamond), lowest $4k_F$ -singlet excitations (plus), and lower (open triangle) and upper (solid triangle) spectrum edges. Lines show dispersions $! (k)$ obtained from the Bethe Ansatz solution.

They give the spectral onset for $k_F < |k_j| < 2k_F$. For $3k_F < |k_j| <$ this onset corresponds to a secondary spinon band with $k_c = -4k_F$ and $|k_s| < k_F$.

In Fig. 3, a dashed line shows the dispersion of the lowest possible excitations made of one spinon and one holon [i.e., the minimum of $!_c(k_c) + !_s(k_s)$ for a given $k = k_c + k_s$]. This lower edge of the spinon-holon continuum is not related to any feature in the DDMRG spectral function and carries spectral weight at lower energy $!$. Therefore, the Hubbard model spectral function can not be explained with spinon-holon excitations only. Actually, the lower edge of the spectrum follows the dispersion of the lowest states made of one spinon and a single charge excitation called $4k_F$ -singlet excitation in Ref. [8]. Finally, the very weak peaks found for $2t > ! > 4t$ and $|k_j| > 2k_F$ seem to be related to the lowest possible $4k_F$ -singlet charge excitations with $k_s = -k_F$ and $k_c k_s > 0$.

In Ref. [5] it was shown that the dispersion of the TCNQ related peaks in the ARPES spectrum of TTF-TCNQ could be mapped onto excitation bands of a one-dimensional Hubbard model. Our DDMRG calculations show that the Hubbard model also explains qualitatively the experimental spectral weight distribution. (A quantitative comparison is not possible because of the strong background contribution in the ARPES data.) The ARPES spectrum features labeled (a), (b), and (d) in Refs. [4, 5] perfectly match the (singular) features found in the Hubbard model spectral function (the spinon, holon, and shadow bands, respectively). This confirms that the ARPES spectrum of TTF-TCNQ shows the signature of spin-charge separation over the scale of the conduction band width (of the order of 1eV). In addition, we note that the secondary holon bands (for $k_F < |k_j| < 2k_F$) correspond to a poorly understood spectral feature [labeled (c)] which has been attributed to excitations of the

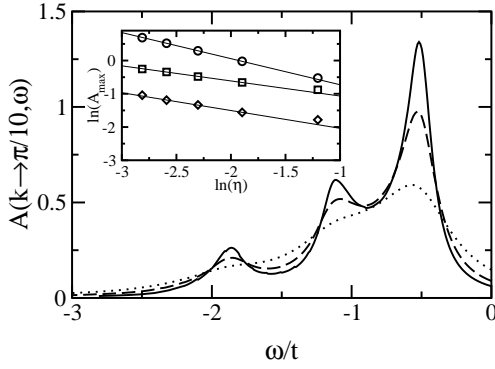


FIG. 4: Spectral functions $A(k \rightarrow \pi/10 = k_F/3; !)$ calculated with DDMRG for system sizes $L = 30$ (dotted), 60 (dashed), and 90 (solid). Inset: scaling of the peak maximum for $0.3 \geq \eta \geq 0.06$ ($30 \leq L \leq 150$). Solid lines are fits.

TTF band in Refs. [4, 5]. Therefore, we think that this spectral feature is not related to the TTF band but is naturally explained by the TCNQ secondary holon bands, at least in the range $k_F < |k| < 2k_F$.

In the Luttinger liquid theory the spectral functions $A(k; !)$ have singularities $|k - k_F|^{-\alpha}$ for energies $(k) / |k - k_F|$ given by the spinon and holon linear dispersions [2, 3]. For a system which is invariant under spin rotation the exponents are related to the Luttinger liquid parameter K through $\alpha_s = (4 - K - K^{-1})/4$ on the spinon branch and $\alpha_c = (6 - K - K^{-1})/8$ on the holon branch. The parameter K can be calculated in the one-dimensional Hubbard model [15] and one finds $K = 0.68$ for $U = 4.9t$ and $n = 0.6$, which corresponds to exponents $\alpha_s = 0.46$ and $\alpha_c = 0.48$.

In view of the Luttinger liquid theory results it is natural to ask whether the broadened peaks found in our DDMRG calculations become singularities of the spectral function in the thermodynamic limit. To answer this question and to estimate the exponents we have performed a finite-size-scaling analysis [14]. The spectral function $A(k; !)$ is calculated for several system sizes L with a broadening scaling as $\eta = 9t/L$. Some spectra for $k \rightarrow \pi/10 = k_F/3$ are shown in Fig. 4. The scaling of the peak maximum A_{max} with η can then be analyzed (see the inset of Fig. 4). If A_{max} diverges as $\eta^{-\alpha}$ ($0 < \alpha < 1$) for $\eta \rightarrow 0$, the spectral function has a singularity with exponent α in the thermodynamic limit. A Landau quasiparticle corresponds to a Dirac δ -function and thus to a peak diverging as η^{-1} .

Using this scaling analysis we have found that the spinon, holon and shadow band peaks become singularities in the thermodynamic limit. We have not found any diverging peak with an exponent larger than 0.86, which confirms the absence of Landau quasiparticles.

For $k \rightarrow \pi/10$ we have found that the spinon, holon, and shadow band exponents are $\alpha_s = 0.78$, 0.44 , and 0.56 , respectively. For $k \rightarrow 0$, we have obtained $\alpha_s = 0.86$ for the spinon band and $\alpha_c = 0.70$ for the holon/shadow band. Therefore, the exponents are momentum-dependent and for finite $|k - k_F|$ they are significantly different from the Luttinger liquid predictions for $|k| \rightarrow k_F$. A recent study [16] has also shown that these exponents are strongly k -dependent. It is not possible to determine the exponents in the asymptotic Luttinger liquid regime with DDMRG because the finite-size effects are not under control in that limit.

In summary, we have used a novel approach to compute the photoemission spectral function of the Hubbard model on open chains using DDMRG and explained the ARPES spectrum of the organic conductor TTF-TCNQ. Our method can easily be extended to other dynamical response functions and more complicated models.

We are grateful to R. Claessen, F. H. L. Essler, and J. Carmelo for helpful discussions. H.B. acknowledges support by the Optodynamics Center of the Philipps-Universität Marburg and thanks the Institute for Strongly Correlated and Complex Systems at Brookhaven National Laboratory for its hospitality.

-
- [1] K. Schonhammer, Luttinger liquids: the basic concepts, to be published in Strong Interactions in Low Dimensions, edited by D. Baeriswyl and L. Degiorgi (Kluwer, 2004); e-print cond-mat/0305035 (unpublished).
 - [2] J. Voit, Phys. Rev. B 47, 6740 (1993).
 - [3] V. Meden and K. Schonhammer, Phys. Rev. B 46, 15753 (1992).
 - [4] R. Claessen et al., Phys. Rev. Lett. 88, 096402 (2002).
 - [5] M. Sing et al., Phys. Rev. B 68, 125111 (2003).
 - [6] J. Hubbard, Proc. R. Soc. London A 276, 238 (1963).
 - [7] E. H. Lieb and F. Y. Wu, Phys. Rev. Lett. 20, 1445 (1968).
 - [8] H. J. Schulz, e-print cond-mat/9302006 (unpublished).
 - [9] K. Penc, K. Hallberg, F. Mila, and H. Shiba, Phys. Rev. Lett. 77, 1390 (1996); Phys. Rev. B 55, 15475 (1997).
 - [10] J. Favand et al., Phys. Rev. B 55, 4859 (1997).
 - [11] R. N. Bannister and N. d'Ambrumenil, Phys. Rev. B 61, 4651 (2000).
 - [12] R. Preuss et al., Phys. Rev. Lett. 73, 732 (1994); M. G. Zacher, E. Arrigoni, W. Hanke, and J. R. Schrieffer, Phys. Rev. B 57, 6370 (1998).
 - [13] D. Senechal, D. Perez, and M. P. Lado-Ladriere, Phys. Rev. Lett. 84, 522 (2000).
 - [14] E. Jeckelmann, Phys. Rev. B 66, 045114 (2002); E. Jeckelmann, F. Gebhard, and F. H. L. Essler, Phys. Rev. Lett. 85, 3910 (2000).
 - [15] H. J. Schulz, Phys. Rev. Lett. 64, 2831 (1990).
 - [16] J. M. P. Carmelo et al., Europhys. Lett. (2004), to be published; e-print cond-mat/0307602 (unpublished).